CAMBRIDGE
UNIVERSITY PRESS

RESEARCH ARTICLE

Fuzzy radial-based impedance controller design for lower limb exoskeleton robot

Peng Zhang[1,2], Junxia Zhang[1,2,*] (ID) and Ahmed Elsabbagh[3]

[1]Tianjin University of Science & Technology, Dagunan Road, Tianjin, China, [2]Tianjin Key Laboratory for Integrated Design and Online Monitor Center of Light Design and Food Engineering Machinery Equipment, Tianjin, China, and [3]School of Design and Production Engineering, Ain shams University, Cairo, Egypt
*Corresponding author: E-mail: zjx@tust.edu.cn

Abstract

The lower extremity rehabilitation exoskeleton is mainly used to help patients with movement disorders complete rehabilitation training. For the human-machine interaction problem of the lower limb rehabilitation exoskeleton, a fuzzy radial-based impedance (RBF-FVI) controller is proposed in this study. A six degree of freedom (DOF) lower extremity rehabilitation exoskeleton was developed, and the human-machine coupling dynamics model was established. To realize the compliance control of the human-machine coupling system, a novel RBF-FVI controller is designed, which includes an inner-loop fuzzy position control module and an outer-loop impedance control module. The inner-loop fuzzy position control module is mainly used to achieve the tracking control of the desired training trajectory and position adjustment amount. The outer-loop impedance control module regulates the impedance parameters and compensates for the uncertainty terms. The superiority of the proposed controller in trajectory following is verified through simulation and comparison tests. The hardware test of the human-machine coupling system was carried out, and the test results showed that the subject and the exoskeleton system could realize a coordinated and smooth movement.

1. Introduction

Neurological injuries, such as stroke, spinal cord injury, and skeletal muscle weakness in the elderly, may largely limit the ability of this population to achieve major activities of daily living [1]. Recently, there has been a growing interest in developing exoskeleton devices, which can help the disabled with motor assistance and rehabilitation training [2, 3]. An exoskeleton robot is usually defined as designed following the shape and function of the body. Exoskeleton robots can effectively integrate the cognitive abilities of humans and the advantages of robotic devices to help users accomplish rehabilitation activities [4].

In recent years, many studies have been conducted to improve the performance of lower extremity exoskeletons [5–7]. As precision and portable exoskeleton designs have evolved, researchers have also focused on improving control strategies to increase exoskeletons' precision, efficiency, and comfort. Since humans wear the exoskeleton, good interaction between the exoskeleton and humans is a key factor, which means the exoskeleton needs to realize compliance control [8]. The lower limb exoskeleton compliance control is mainly divided into two categories, one is passive compliance control and the other is active compliance control. Passive compliance control is to install some cushioning devices (such as springs) on the exoskeleton to absorb or relieve the impact energy between the exoskeleton and humans during the movement [9, 10]. Active compliance control means that the robot uses the force feedback information and adopts a certain control strategy to actively control the force [11]. The Swiss Lokomat lower extremity rehabilitation exoskeleton uses a hybrid force/position adaptive control strategy in active rehabilitation [12, 13]. The hybrid force/position control strategy utilizes dual force and

position control to realize compliance rehabilitation training. The ALEX lower limb exoskeleton also employs a hybrid force/position control strategy, allowing this lower limb exoskeleton to achieve desired gait planning while applying less force on the wearer's leg [14]. However, this method requires a very accurate model of the robot dynamics. And the hybrid force/position control requires real-time detection of force and position changes, so many sensors need to be installed. Impedance control has been widely used to realize compliance control by adjusting the dynamic relationship between the human-machine position and the interacting force [15–18]. The Ekso lower limb exoskeleton used an impedance control strategy based on a force field controller, which firstly sets the desired motion trajectory and then corrects the gait trajectory by detecting the interactive forces between the human and the machine [15]. Chen designed an impedance control strategy with a perturbation observer for the exoskeleton robot system. The experimental results show that the exoskeleton could actively adjust the motion trajectory when encountering obstacles and accurately track human motion trajectory [16].

In the actual use of the process, the state of the robot and external disturbances are random. Hence, impedance control with fixed impedance parameters cannot adapt to the unstable motion environment. With the development of science and technology, intelligent algorithms are increasingly used to assist impedance control for active control [19–25]. Majied proposed a novel hybrid optimized adaptive sliding mode impedance control method for a lower limb exoskeleton robot with seven active joints. The simulation results reveal the superiority of the controller in comparison with SMC [19]. To improve human-machine coordination, Chen proposed an improved impedance control strategy based on a genetic algorithm to follow the tracking trajectory. Compared with the traditional method, the impedance parameters can be calculated and adjusted online, and the gait trajectory can be well tracked [20]. However, this study is still in the simulation test stage, and the effectiveness of the application to the hardware platform needs to be further verified. A time-varying desired impedance model based on the wearer's lower extremity motility is proposed to provide appropriate power and balance assistance during sit-to-stand movements. The effectiveness of the method was verified through experiments with four healthy subjects. Good results were obtained regarding reasonable power assistance and balance reinforcement [21]. Akdoğan, Erhan designed an adaptive impedance control system for a knee rehabilitation robot using the interaction forces between the knee joint and the robot [23]. The experimental results showed that real-time adjustment of the target impedance parameters could effectively regulate the active release forces of the knee joint. However, it still has some limitations in complex rehabilitation training behaviors.

Although the conventional impedance control method has achieved some good results, the performance of the whole system still depends on the manual selection of the target impedance control parameters. And the effect of existing compliance control algorithms is not ideal. In this study, a fuzzy radial-based impedance (RBF-FVI) controller is presented to realize compliance control. The main contributions of the paper are:

1. A 6 degree of freedom (DOFs) lower limb exoskeleton robot was designed. The hip and knee of each artificial leg can provide two electric-powered DOFs for flexion/extension. And two passive-installed DOFs of the ankle were used to achieve the motion of supination /overpronation and plantarflexion/dorsiflexion. The human-machine coupled dynamics equations based on the spring-damping model are established, and the object under study is determined.

2. To meet the rehabilitation training needs of patients based on conforming to the laws of human movement, this paper proposes an RBF-FVI controller, which includes a fuzzy position control module and an outer-loop impedance control module. The fuzzy position control module is mainly used to control the desired training trajectory tracking and the position adjustment amount. The external loop impedance control module can establish the dynamic force/position relationship between the subject and the exoskeleton, enabling the patient to adjust the gait trajectory autonomously in real-time to improve the suppleness of human-machine interaction.
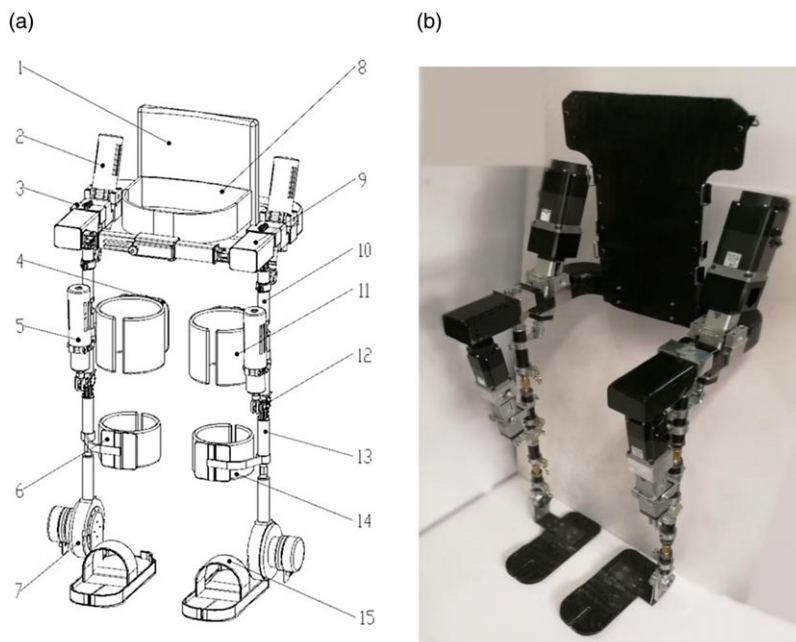
Figure 1. *(a) Overall structure diagram (1) Back support; (2) Driving source of hip joint; (3) Hip joint component; (4) Brace of thigh; (5) Driving source of knee joint; (6) Brace of calf; (7) Ankle joint component; (8) Flexible belt of waist; (9) Waist component; (10) Thigh component; (11) Flexible belt of thigh; (12) Knee joint component; (13) Calf component; (14) Flexible belt of calf; (15) Pedal; (b). Exoskeleton mechanical diagram.*

3. Simulation experiments are performed on the joint platform of MATLAB/Simulink and ADAMS. The performance is also analyzed in comparison with the conventional control algorithm. The hardware tests of the exoskeleton robot system were conducted. The test results show that the robot system's safety control and impedance control can be achieved, and the operator and the exoskeleton robot can realize cooperative movement.

The rest of the paper is organized as follows: Section 2 describes exoskeleton robot system. Section 3 illustrates the design of RBF-FVI controller. The simulation experiment and analysis are presented in Section 4. Section 5 describes human-machine coupling test. Finally, the conclusion of this work is given in Section 6.

2. Exoskeleton robot system

2.1. Structure of exoskeleton robot

The developed lower limb exoskeleton is shown in Fig. 1. The exoskeleton robot designed in this paper mainly considers the motion in the sagittal plane. For each leg, it has one active DoF for the hip joint and knee joint, respectively, and one passive DoF for the ankle joint.

Each leg will alternate into the support phase and the swing phase. The lower limb exoskeleton control system mainly considers the following ability of the human lower limb motion and the magnitude of the interaction force during the motion. Therefore, in this paper, the dynamics of the swing phase are modeled. The single leg of the lower limb exoskeleton is simplified to a duplex structure consisting of the hip and knee joints as well as the thigh and calf rods. A simplified model of the swing phase of the lower limb exoskeleton was established, as shown in Fig. 2(a). The hip joint is taken as the origin
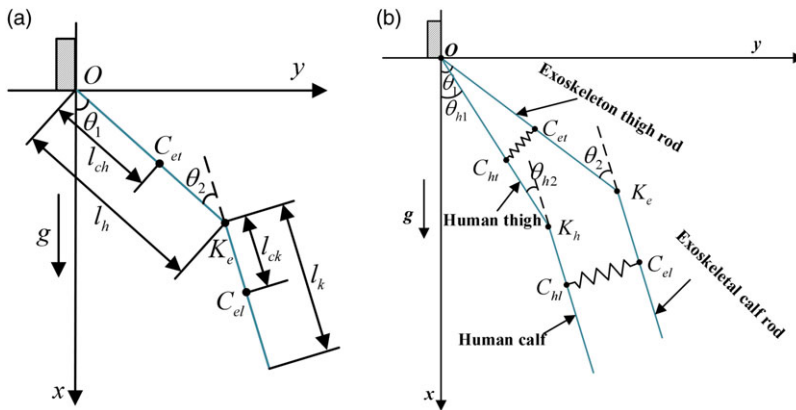
Figure 2. *(a) Simplified model of lower extremity exoskeleton in swing phase; (b)Human-machine coupling system model.*

of the coordinate system. The point O is the hip joint of the exoskeleton, K_e is the knee joint of the exoskeleton, C_{et} is center of mass of the thigh rod, C_{el} is the center of mass of the calf rod, the mass of the thigh rod is m_{eh}, the mass of the calf rod is m_{ek}, the length of the thigh rod is l_h, the length of the calf rod is l_k, the distance from the C_{et} to the point O is l_{ch}, the distance from the C_{el} to the knee joint is l_{ck}, the rotational inertia of the thigh rod is I_{eh}, the rotational inertia of the calf rod is I_{ek}. The angle between the thigh rod and the vertical direction is θ_1. The angle between the calf bar and the thigh bar is θ_2. The counterclockwise direction is specified as the positive direction.

The exoskeleton robot dynamics equation is:

$$\tau = M(\theta)\,\ddot{\theta} + C(\theta,\dot{\theta})\,\dot{\theta} + G(\theta) \tag{1}$$

where $\theta, \dot{\theta}, \ddot{\theta}$ are 2×1 order lower limb exoskeleton joint angle, velocity and acceleration, respectively; $M(\theta)$ is 2×2 order inertia matrix; $C(\theta,\dot{\theta})$ is 2×2 order Coriolis force matrix; $G(\theta)$ is 2×1 order gravity matrix; τ is 2×1 order joint driving force matrix. The joint torque can be obtained from the torque sensor.

The joint torque is:

$$\tau = \begin{bmatrix} \tau_1 \\ \tau_2 \end{bmatrix} \tag{2}$$

where τ_1 and τ_2 are the torque of hip joint and knee joint, respectively.

According to Lagrange dynamic equation, the calculation of the generalized torque of the hip joint and knee joint are:

$$\tau_1 = \frac{d}{dt}\frac{\partial L}{\partial \dot{\theta}_1} - \frac{\partial L}{\partial \theta_1} = m_{eh}l_{ch}^2\ddot{\theta}_1 + l_h\ddot{\theta}_1 + m_k l_h^2\ddot{\theta}_1 + m_k l_{ck}^2\ddot{\theta}_1 + I_{ek}(\ddot{\theta}_1 + \ddot{\theta}_2)$$
$$+ m_{ek}l_{ck}^2\ddot{\theta} + 2m_k l_h l_{ck}(\ddot{\theta}_1 \cos\theta_2 - \dot{\theta}_1\dot{\theta}_2 \sin\theta_2) + m_{ek}l_h l_{ck}(\ddot{\theta}_2 \cos\theta_2 - \dot{\theta}_2^2 \sin\theta_2) + m_{eh}gl_{ch} \sin\theta_1$$
$$+ m_{ek}g(l_h \sin\theta_1 + l_{ck} \sin(\theta_1 + \theta_2)) \tag{3}$$

$$\tau_2 = \frac{d}{dt}\frac{\partial L}{\partial \dot{\theta}_2} - \frac{\partial L}{\partial \theta_2} = \left(m_{ek}l_{ck}^2 + I_{ek}\right)(\ddot{\theta}_1 + \ddot{\theta}_2) + m_{ek}l_h l_{ck}(\ddot{\theta}_1 \cos\theta_2 - \dot{\theta}_1\dot{\theta}_2 \sin\theta_2)$$
$$+ m_{ek}l_h l_{ck}\dot{\theta}_1(\dot{\theta}_1 + \dot{\theta}_2)\sin\theta_2 + m_{ek}gl_{ck}\sin(\theta_1 + \theta_2) \tag{4}$$

The design of the power system adopts the linear actuator of servo motor and ball screw, and its motion mode is similar to human lower limb skeletal muscle. The relationship between output torque of

servo motor and thrust of the ball screw is:

$$\tau_m = \frac{F \times L}{2 \times \pi \times \eta} \tag{5}$$

where τ_m is output torque of servo motor, F is thrust force of ball screw, L is the telescopic length of the ball screw, η is transmission efficiency from motor to ball screw.

2.2. Human-machine interaction torque

The human lower limb and the exoskeleton are bundled together, and there is always an interaction torque between the two during the moving process. The human-machine coupled system model in the swing phase is shown in Fig. 2(b). It is assumed that the thigh and calf rods of the exoskeleton are the same length as the human thigh and calf, respectively, and the center of mass is also in the same position. K_h is the human knee joint, C_{ht} and C_{hl} are the center of mass human thigh and human calf, respectively. The mass of human thigh is m_{hh}, the mass of human calf is m_{hk}.

$$\tau_{dis} = \begin{bmatrix} \tau_{dis1} \\ \tau_{dis2} \end{bmatrix} \tag{6}$$

$$\tau_{dis1} = K_{imp}(\theta_{h1} - \theta_1) \tag{7}$$

$$\tau_{dis2} = K_{imp}(\theta_{h2} - \theta_2) \tag{8}$$

where τ_{dis1} and τ_{dis2} are human-machine interaction torque of hip joint and knee joint, respectively. K_{imp} is the elasticity coefficient between the human and the exoskeleton, and $K_{imp} = 17$ N·m/rad. θ_{h1} and θ_{h2} are the rotation angle of human hip joint and knee joint, respectively.

3. Fuzzy radial-based impedance controller design

3.1. Overall structure

In the whole rehabilitation training process, to meet the patient's rehabilitation needs based on human movement patterns, this paper proposes an RBF-FVI control algorithm. The proposed control strategy mainly consists of an inner-loop fuzzy position control module and an outer-loop impedance control module, as shown in Fig. 3.

3.2. Inner-loop fuzzy PID position control module

The fuzzy position control module is mainly used to realize the tracking control of the desired training trajectory and position adjustment. $e(t)$ and $u(t)$ represent the input and output of the PID controller, respectively. $\Delta\theta$, $\Delta\dot{\theta}$ are the input variables of the fuzzy control rules. $\Delta\tau$ is the force error. τ_m is the output torque. K_p, K_i, and K_d are the proportional, integral and differential gains. θ_e and θ_d are the actual and desired positions of the end of the exoskeleton, respectively. τ_d are the desired torque. $B(t)$, $K(t)$, and $M(t)$ denote the amount of damping parameter, stiffness parameter, and inertia parameter, respectively.

Conventional PID controller was able to dynamically adjust the relationship between force and position. But it is still difficult to satisfy complex nonlinear and strongly coupled systems, such as exoskeleton robots. However, fuzzy PID control does not require an accurate mathematical model. The fuzzy mathematical theory and methods can be used to adjust the PID parameters in real-time to achieve optimal control [26, 27]. In order to realize the parameter adaptive control, the input is the position error $\Delta\theta$ and the change rate of position error $\Delta\dot{\theta}$, and the output is the real-time adjusted parameters K_p, K_i, and K_d. When the joint angle increases, it is set to a positive value, and when it decreases, it is set to a negative value. The fuzzy rule of K_p is used for illustration. The learning rate adjustment principle of K_p
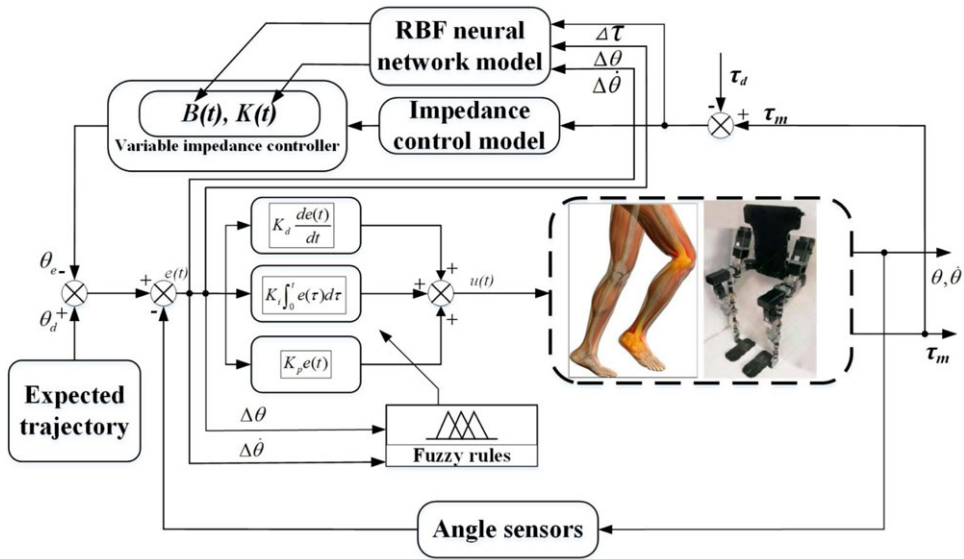
Figure 3. *Overview chart of RBF-FVI controller.*

is summarized as follows: In the PID controller, the selection of K_p value is determined by the system's response speed. Increasing K_p can improve the response speed and reduce the steady-state deviation; however, too large a K_p value will produce a large overshoot and make the system unstable. Therefore, a larger K_p value should be taken at the beginning of regulation to improve the response speed, while in the middle of regulation, K_p is taken as a smaller value to make the system have a smaller overshoot and ensure a certain response speed; while in the late regulation process, K_p is adjusted to a larger value to reduce the static difference and improve the control accuracy. The fuzzy sets of both input and output variables are set to seven groups, which are NB (negative large), NM (negative medium), NS (negative small), ZO (zero), PS (positive small), PM (positive medium), and PB (positive large). This sets an extremely large number of levels, and the rules are formulated flexibly and carefully to adapt to control under different conditions. The setting fuzzy control rules are shown in Table I.

3.3. Outer-loop neural network regulation impedance parameter module

The outer-loop impedance control was used to regulate the impedance parameters and compensate for uncertainty. The adjustment amount of the movement trajectory was obtained through the human-machine interaction force so that the movement of the rehabilitation robot can actively adapt to the movement intention of the patient and realize the active compliance of the movement function rehabilitation training. The human-machine interaction force can be calculated by solving the difference between the measured value of the torque sensor installed at the robot joint and the value calculated by the dynamic model of the human-machine coupling system. Through inverse kinematics, the reference trajectory in Cartesian space can be converted into a reference trajectory in joint space. Then, the corrected reference trajectory can be used as a reference trajectory, reflecting the patient's active motion intention.

3.3.1. Impedance control

Instead of directly controlling the magnitude of the force between exoskeleton robot and human, impedance controller controls the robot system by establishing the relationship between the force and position error. There have been many studies using impedance control methods to control exoskeleton

Table I. *The fuzzy control rules for K_p.*

K_p		$\Delta\theta$						
		NB	**NM**	**NS**	**ZO**	**PS**	**PM**	**PB**
$\Delta\dot{\theta}$	NB	NB	NB	NM	NM	NS	ZO	ZO
	NM	NB	NB	NM	NS	NS	ZO	ZO
	NS	NM	NM	NS	NS	ZO	PS	PS
	ZO	NM	NS	NS	ZO	PS	PS	PM
	PS	NS	NS	ZO	PS	PS	PM	PB
	PM	ZO	ZO	PS	PS	PM	PB	PB
	PB	ZO	ZO	PS	PM	PM	PB	PB
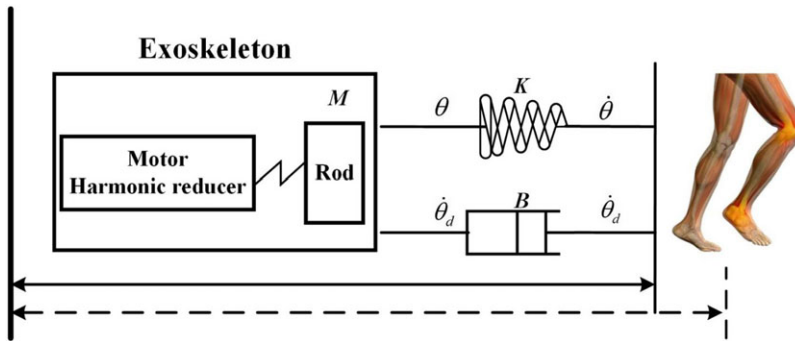
Figure 4. *Impedance control model.*

robots for multiple motion tasks [28, 29]. A second-order differential equation is usually used to represent the impedance model of the exoskeleton robot, which can be expressed as a mass-spring-damping system, as shown in Fig. 4.

The target impedance is

$$\tau = M(\ddot{\theta}_d - \ddot{\theta}) + B(\dot{\theta}_d - \dot{\theta}) + K(\theta_d - \theta) \tag{9}$$

where τ is the interaction torque between human and exoskeleton robot, M is the impedance inertia matrix, B is the impedance damping matrix, K is the impedance stiffness matrix. $\theta_d, \dot{\theta}_d, \ddot{\theta}_d$ are the position, velocity, and acceleration of human in Cartesian space. $\theta, \dot{\theta}, \ddot{\theta}$ are the position, velocity, and acceleration of exoskeleton robot in Cartesian space.

Impedance control successfully accommodates position control and force control into a dynamic framework that allows position and force to satisfy desired dynamic relationship [30]. There are two main types of impedance control, namely force-based impedance control and position-based impedance control. Compared with force-based impedance control, the position-based impedance control does not need to establish a very accurate dynamics model, and the position-based impedance control theory is more mature and superior in terms of stability and accuracy. Therefore, this paper adopts position-based impedance control to optimize the design of the exoskeleton robot torque feedback control system. Position-based impedance control obtains the position to be compensated by calculating the human-machine contact force deviation. The compensation force is converted to joint compensation angle.

For single joint, when there is a deviation between the actual position of the joint and the operator's position, the actual contact force is calculated by the position deviation and contact stiffness. The desired position of the exoskeleton joint is:

$$\widetilde{\theta}_d = \theta_d - \theta_{ref} \tag{10}$$

where θ_d is desired human joint angle. θ_{ref} is impedance compensation angle.
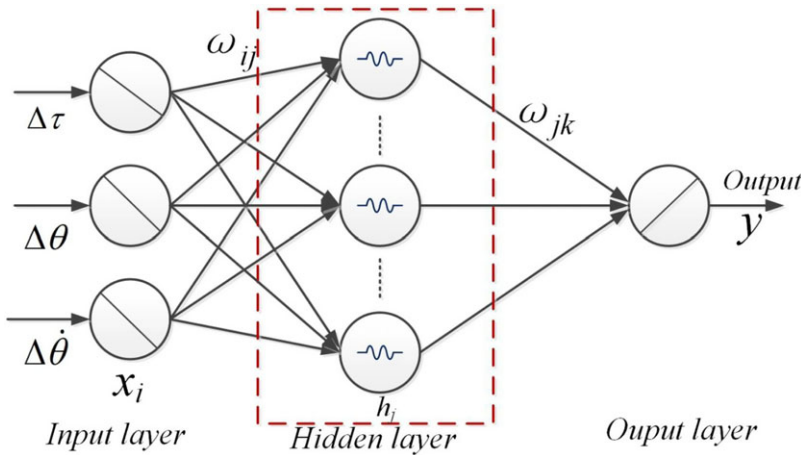
Figure 5. *Structure diagram of RBF neural network.*

Let $\theta_e = \widetilde{\theta}_d - \theta$, the position control is calculated as:

$$\tau - \tau_{pd} = \hat{M}(\theta_d)\,\ddot{\widetilde{\theta}}_d + \hat{C}\left(\widetilde{\theta}_d, \dot{\widetilde{\theta}}_d\right)\dot{\widetilde{\theta}}_d + \hat{G}(\widetilde{\theta}_d) \tag{11}$$

$$\tau_{pd} = K_p\theta_e + K_d\frac{d\theta_e}{dt} \tag{12}$$

where θ is actual exoskeleton joint angle. τ_{pd} is compensation torque from PID feedback control. $\hat{M}(\theta)$, $\hat{C}(\theta, \dot{\theta})$ and $\hat{G}(\theta)$ are the ideal inertia matrix, damping parameter matrix, and gravity matrix of the exoskeleton robot.

3.3.2. Radial basis function (RBF) neural network

The RBF neural network is a three-layer neural network with an input layer, a hidden layer, and an output layer [31]. The transformation between the input layer to the hidden layer is nonlinear. The transformation from the hidden layer to the output layer is linear. The RBF neural network has a fast learning speed and is suitable for real-time control systems. In this study, the RBF neural network model was used to adjust the target impedance parameters in real-time and compensate for the model's uncertainty. Based on the traditional impedance control, the RBF neural network algorithm is used to adjust the impedance parameters in real time to improve the stability and flexibility of the control algorithm to achieve better control results. The structure of the RBF neural network is shown in Fig. 5.

The input layer of the RBF neural network is the vector x_i. When the inputs are different, the adjusted impedance parameters are also different. When the input is position error $\Delta\theta$ and force error $\Delta\tau$, the output variable is the stiffness correction ΔK. The hidden layer of the RBF neural network is described as:

$$x_j = \sum_{i=1}^{m}\sum_{j=1}^{l}\omega_{ij}s_j = \sum_{j=1}^{l}\left(\omega_{1j}\Delta\tau + \omega_{2j}\Delta\dot{\theta}\right) \tag{13}$$

When the input is velocity error $\Delta\dot{\theta}$ and force error $\Delta\tau$, the output variable is the damping correction ΔB.

$$x_j = \sum_{i=1}^{m}\sum_{j=1}^{l}\omega_{ij}s_j = \sum_{j=1}^{l}\left(\omega_{1j}\Delta\tau + \omega_{2j}\Delta\dot{\theta}\right) \tag{14}$$

$$d_j = f(x_j) \tag{15}$$

where *m* denotes the number of input variables; the RBF neural network designed in this paper has two input variables, that is, $m = 2$. s_j and d_j are the input and output of the hidden layer neural network nodes, respectively, and ω_{ij} is the weighting coefficient between the input layer and the hidden layer.

The activation function of the hidden layer neuron is:

$$f(x_j) = \exp\left(-\|x_j - c_j\|^2 / (2b_j^2)\right), j = 1, 2, \ldots, l \tag{16}$$

where c_j is the center of the basis function. b_j is the width of the basis function. l is the number of nodes in the hidden layer.

The output layer of the RBF neural network is described as:

$$y = \omega_{jk}d_j + f \tag{17}$$

$$y_m = \omega_{jk}d_j \tag{18}$$

where f is modeling error and external perturbation. y is the output value of the RBF network in the presence of the disturbance term f. y_m is the output value of the RBF network without f. ω_{jk} is the weighting coefficient between the hidden layer and the output layer.

The supervised learning method was used to train all parameters of the RBF neural network (center of RBF c_j, variance b_j, and weights between the hidden layer to the output layer ω_{jk}). This is mainly done by performing gradient descent on the cost function and then correcting each parameters. Specifically, firstly, the parameters of RBF neural network are initialized randomly; then, the supervised training optimization is performed by gradient descent for all three parameters in the network. The cost function was set as:

$$E = \frac{1}{2}(y - y_m)^2 \tag{19}$$

Then in each iteration, the parameters are adjusted at a certain learning rate in the negative direction of the error gradient until the best parameter values are obtained.

$$c_{ij}(t) = c_{ij}(t-1) - \eta \frac{\partial E}{\partial c_{ij}(t-1)} + \alpha\left[c_{ij}(t-1) - c_{ij}(t-2)\right] \tag{20}$$

$$b_{ij}(t) = b_{ij}(t-1) - \eta \frac{\partial E}{\partial b_{ij}(t-1)} + \alpha\left[b_{ij}(t-1) - b_{ij}(t-2)\right] \tag{21}$$

$$\omega_{jk}(t) = \omega_{jk}(t-1) - \eta \frac{\partial E}{\partial \omega_{jk}(t-1)} + \alpha\left[\omega_{jk}(t-1) - \omega_{jk}(t-2)\right] \tag{22}$$

where $c_{ij}(t)$ is the central component of the i_{th} hidden layer neuron for the j_{th} input neuron at the t times iteration; $b_{ij}(t)$ is the width vector of the neuron corresponding to $c_{ij}(t)$; $\omega_{jk}(t)$ is the conditioning weight between the j_{th} output neuron and the k_{th} hidden layer neuron at the t times iteration of computation. η is learning rate, $\eta = 0.8$. α is the momentum factor, $\alpha = 0.5$.

3.4. Stability analysis

The Laypunov function was selected as:

$$V = X^T P X + \|\widetilde{\omega}_{jk}\|_F^2 \tag{23}$$

There exists a positive definite matrix P, satisfying $A^T P + PA = -Q$.
where Q is a given positive definite symmetric matrix.

$$\widetilde{\omega}_{jk} = \omega_{jk}^* - \hat{\omega}_{jk} \tag{24}$$

where ω_{jk}^* is actual weight of RBF neural network, $\hat{\omega}_{jk}$ the estimated value of the weight.

Based on the theory of stability analysis of control systems, it is defined as:

$$\left\|\omega_{jk}\right\|_{\mathrm{F}}^2 = tr\left(\widetilde{\omega}_{jk}{}^T\widetilde{\omega}_{jk}\right) \geq 0 \tag{25}$$

where $tr()$ is the trace of the matrix.

The modeling error and external perturbation f are described as:

$$f = \hat{\omega}_{jk}\varphi(x_j) \tag{26}$$

where $\phi(x_j)$ is the output of the Gaussian basis function, and $\varphi(x_j) = [f(x_1), f(x_2), \ldots f(x_j), \ldots f(x_l)]$.

The error state equation of the system is given by

$$\dot{X} = AX + B\left[f - \hat{f}(x, \omega_{jk})\right] \tag{27}$$

where $X = \begin{bmatrix} e \\ \dot{e} \end{bmatrix}$, $A = \begin{bmatrix} 0 & I \\ K_p & K_d \end{bmatrix}$, $B = \begin{bmatrix} 0 \\ I \end{bmatrix}$, $\hat{f}$ is the estimated value of f.

The relevant term in Eq. (27) is transformed as:

$$f - \hat{f}(x, \omega_{jk}) = f - \hat{f}(x, \omega_{jk}{}^*) + f(x, \omega_{jk}{}^*) - \hat{f}(x, \omega_{jk}) = \beta + \omega_{jk}{}^{*T}\varphi(x_j) - \hat{\omega}_{jk}^T\varphi(x_j) = \beta + \hat{\omega}_{jk}^T\varphi(x_j) \tag{28}$$

where β is the modeling error of the RBF neural network.

$$\dot{X} = AX + B\left(\beta + \hat{\omega}_{jk}{}^T\varphi(x_j)\right) \tag{29}$$

Then,

$$\dot{V} = X^T P\dot{X} + \dot{X}^T PX + 2tr\left(\dot{\widetilde{\omega}}_{jk}{}^T\widetilde{\omega}_{jk}\right) = X^T P\left[AX + B\left(\beta + \widetilde{\omega}_{jk}{}^T\varphi(x_j)\right)\right]^T PX + 2tr\left(\dot{\widetilde{\omega}}_{jk}{}^T\widetilde{\omega}_{jk}\right) \tag{30}$$

Substitute Eq. (27) into Eq. (30) to obtain

$$\dot{V} = -X^T QX + \varphi^T(x_j)\widetilde{\omega}_{jk}B^T PX + \beta^T B^T PX + 2tr\left(\dot{\widetilde{\omega}}_{jk}^T\widetilde{\omega}_{jk}\right) \tag{31}$$

The adaptive rate is taken to be

$$\dot{\widetilde{\omega}}_{jk} = \varphi(x_j)X^T PB - k_1\left\|X\right\|\widetilde{\omega}_{jk} \tag{32}$$

where $k_1\left\|X\right\|$ is the robust term, $k_1 > 0$, and satisfies $\left[B^T PX\varphi^T(x_j) - k_1\left\|X\right\|\right]\widetilde{\omega}_{jk} + \dot{\widetilde{\omega}}_{jk}^T\widetilde{\omega}_{jk} = 0$.

Then,

$$\dot{V} = -X^T QX + 2k_1\left\|X\right\|tr\left[\left(\dot{\widetilde{\omega}}_{jk}^T\widetilde{\omega}_{jk}\right)\right] + 2\beta^T B^T PX \tag{33}$$

According to the parametric property, it is obtained that

$$tr\left(\dot{\widetilde{\omega}}_{jk}^T\widetilde{\omega}_{jk}\right) \leq \left\|\widetilde{\omega}_{jk}\right\|_F\left\|\hat{\omega}_{jk}\right\|_F - \left\|\hat{\omega}_{jk}\right\|_F^2 \tag{34}$$

Then,

$$\dot{V} \leq -X^T QX + 2k_1\left\|X\right\|\left(\left\|\widetilde{\omega}_{jk}\right\|_F\left\|\hat{\omega}_{jk}\right\|_F - \left\|\hat{\omega}_{jk}\right\|_F^2\right) + 2\beta^T B^T PX \leq -\lambda_{\min}(Q)\left\|X\right\|^2$$

$$+ k_1\left\|X\right\|\left(\left\|\widetilde{\omega}_{jk}\right\|_F\left\|\hat{\omega}_{jk}\right\|_F^2\right) + 2\lambda_{\max}(P)\left\|\beta_0\right\|\left\|X\right\|$$

$$= -\left\|X\right\|\left[\lambda_{\min}(Q)\left\|X\right\| + k_1\left[\left\|\widetilde{\omega}_{jk}\right\|_F - \frac{(\omega_{jk})_{\max}}{2}\right]^2 - \frac{k_1}{4}(\omega_{jk})_{\max}^2 - \left\|\beta_0\right\|\lambda_{\max}(P)\right] \tag{35}$$

where $\lambda_{min}(Q)$ is the minimum eigenvalue of matrix Q and $\lambda_{max}(P)$ is the maximum eigenvalue of matrix P.
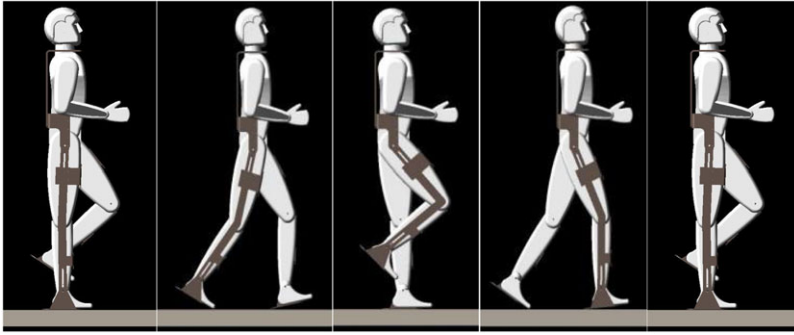
Figure 6. *Simulation process of human-machine coupling model.*
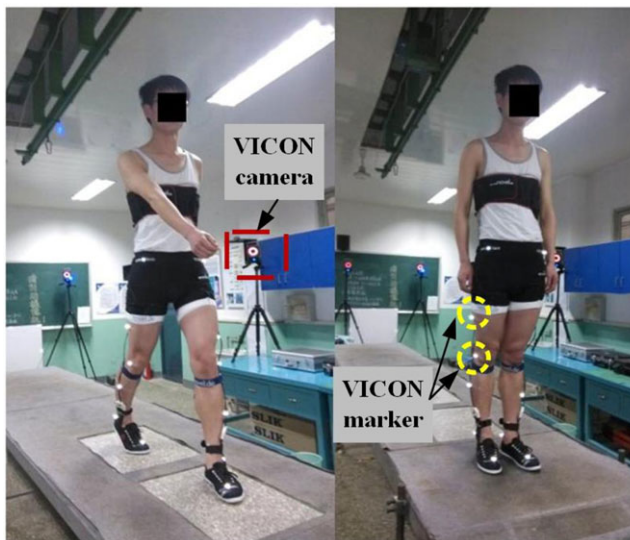

Figure 7. *Gait experiment diagram.*

For $\dot{V} \leq 0$, the following conditions need to be satisfied.

$$\lambda_{\min}(Q)\|X\| \geq \frac{k_1}{4}\left(\omega_{jk}\right)^2_{\max} + \|\beta_0\|\,\lambda_{\max}(P) \tag{36}$$

4. Simulation analysis

4.1. Parameters setting

A human model with 170 cm height and 70 kg weight was set as the study subject, whose thigh length was about 380 mm, calf-length approximately 400 mm, and ankle height about 80 mm. The motion simulation process is shown in Fig. 6. The input of joint trajectories was obtained by human gait experiments. A healthy subject with the age of 25, the weight of 70 kg, and the height of 170 cm is recruited for the experiment, just as shown in Fig. 7. Before the gait experiment, all subjects were given a detailed explanation of the test content and signed a consent form for voluntary participation in the experiment. The subjects had no surgery, no history of lower extremity trauma, no balance problems, or neural muscular disorders within the past six months. A written consent is obtained from the subject. The test environment was a linear walkway of 5 m in length and 1 m in width. The kinematic parameters

Table II. *The parameters of each controller.*

Method	Parameters
Torque feedback	$K_p = 1.5, K_i = 0, K_d = 3$
Impedance controller	$B = 0.5, M = 2, K = 100$
FVI controller	$e \in (1.5, 1.5), e_c \in (-0.5, 0.5), B_0 = 0.2,$
	$M_0 = 2, K_0 = 100; \Delta B \in (-0.5, 0.5),$
	$\Delta M \in (-5, 5), \Delta K \in (-150, 150),$

were acquired by VICON acquisition system(Oxford Metrics Ltd, Oxford, UK). The data acquisition frequency is 1200 Hz.

To verify the effectiveness and superiority of the proposed method, the simulation results are compared with those of torque feedback controller [32], impedance controller [33], and FVI controller [34]. And the parameters of each control method are set, as shown in Table II. The excellent agreement between the reference trajectory and the actual trajectory illustrates the effectiveness of the measurement and control methods.

The RBF neural network includes three layers. The input layer contains two nodes with hip error function and knee error function; the hidden layer uses Gaussian basis function as the excitation function, the center vector is $[-2 \; -1 \; 0 \; 1 \; 2]$, and the width is 0.5; the adaptive rate is taken as 30. The root mean square accuracy was set to 0.01 as the termination condition of the RBF neural network. The moment coefficient of 0.8 is selected, and the simulation is performed at a speed of 0.2 m/s.

4.2. Simulation results analysis

The joint trajectory tracking results of each controller and trajectory error results are shown in Figs. 8, 9, 10 and 11, respectively. When the traditional torque feedback control method was used to perform the motion mission, the maximum error values of the hip joint and knee joint between the exoskeleton robot and the human were 7.8 and 15.1 deg, respectively. Due to the large weight-bearing ratio of the limb, the release of human muscle force has more excellent resistance, so the tracking performance of the human joint position to the exoskeleton robot joint position is poor, and the two have a significant error. The angle deviation needs to be reduced by impedance relationship adjustment. Compared with the torque feedback control system without the impedance control adjustment module, the exoskeleton robot obtained by impedance control has a smaller range of error in the joint angle with the human model. The maximum error of the exoskeleton robot and human hip joint angle is 4.3 deg. This indicates that the exoskeleton robot control system converts the interaction force difference into angular deviation according to the change of human-machine contact force and adjusts the input torque in real-time. The exoskeleton robot provides greater torque support during the limb muscle strength deficiency phase and improves human tracking performance. The maximum angle error values of the hip joint and knee joint obtained based on the fuzzy impedance control method were 3.2 and 9.2 deg, respectively. The error range of the joint angle between the exoskeleton robot and human model is smaller, indicating that the impedance controller with real-time adjustment of impedance parameters improves the control system's control accuracy and the human-machine coupling suppleness better. After adding the neural network error compensation function module, the maximum angle error values of the hip joint and knee joint were reduced to 2.4 and 2.2 deg, respectively. This indicates that the neural network compensation has a good suppression effect on the uncertainty term of the system.

5. Human-machine coupling experiments

5.1. Experimental platform

Human-machine coupling experiments are conducted to demonstrate the functionality of the proposed control method. The exoskeleton robot platform is shown in Fig. 12. The joint motion range of the
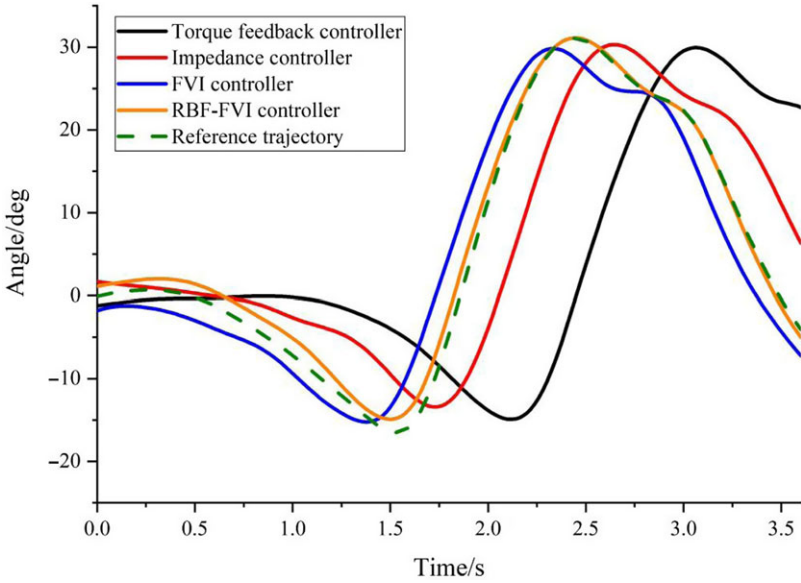
Figure 8. *Hip trajectory tracking results of each controllers.*
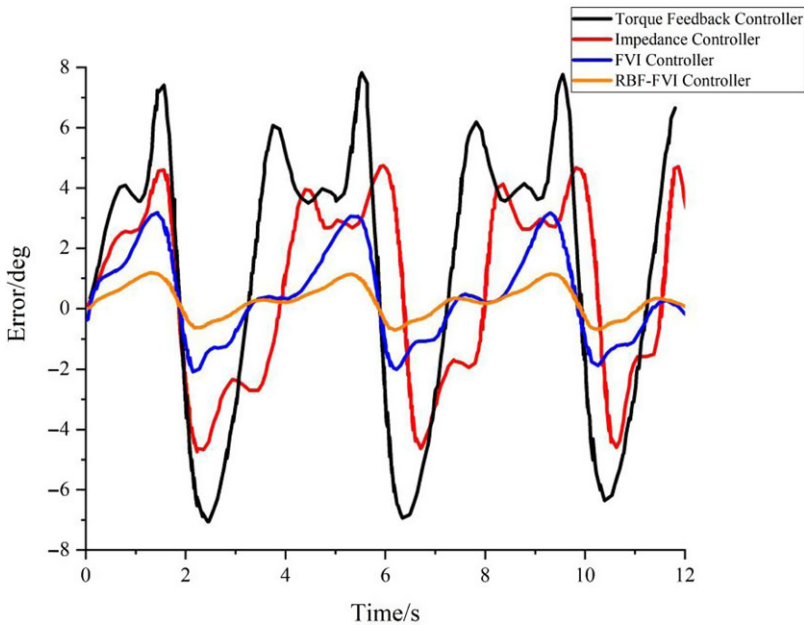

Figure 9. *Trajectory error results of hip joint.*

exoskeleton is 20° flexion and 40° extension for the hip joint, and 70° flexion and 0° extension for the knee joints, and 0° plantarflexion and 20° dorsiflex for ankle joints. The control system consists of the data processor Raspberry Pi and the motion controller STM32F103. Raspberry Pi is used to process data collected from angle sensors (AD36/1217AF. ORBVB, Hengstler, Germany) and torque sensors(TRX-50N·m, Italy). The communication mode between the data processor and motion controller is parallel port communication. The motion controller controls the motors through the controller area network Fieldbus. A healthy subject with the age of 25, the weight of 68 kg, and the height of 170 cm is recruited for the experiment. A written consent is obtained from the subject. For safety reasons, if the angle of
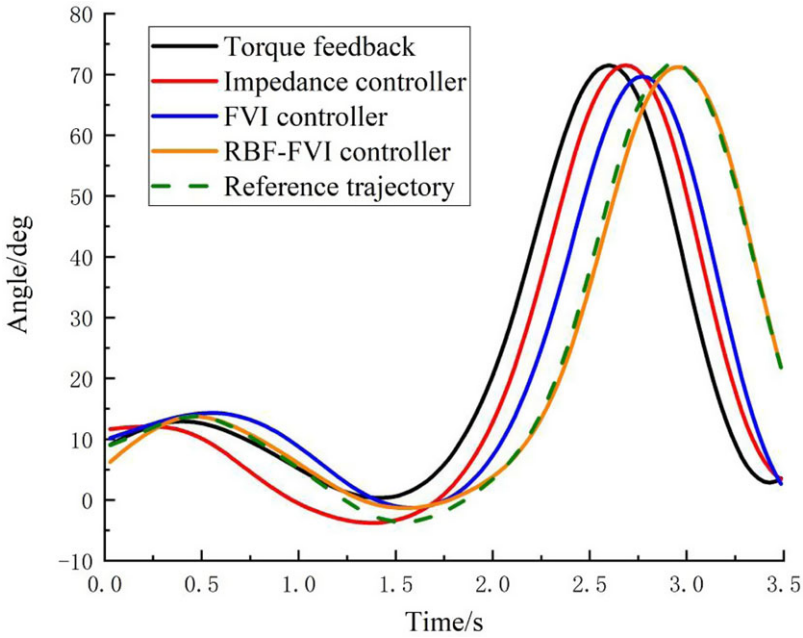
Figure 10. Knee trajectory tracking results of each controllers.
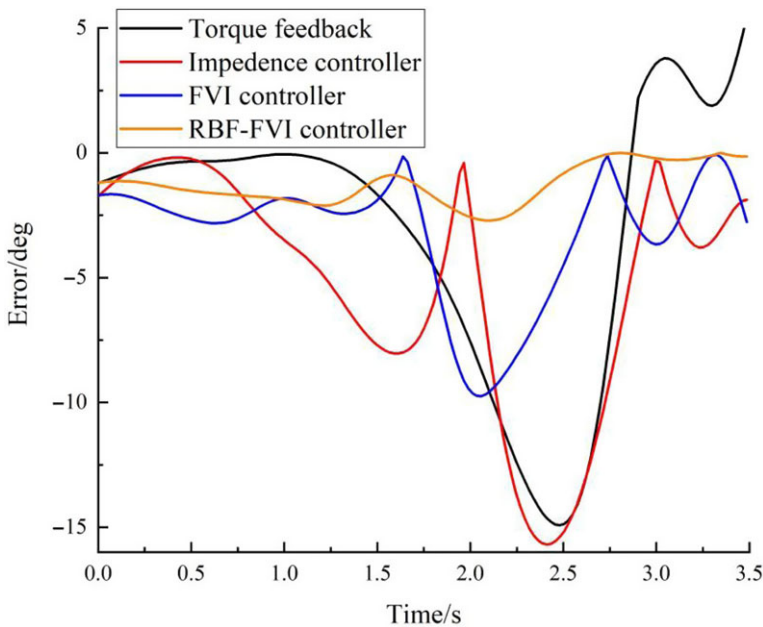
Figure 11. Trajectory error results of knee joint.

the exoskeleton is greater than the allowable value, the exoskeleton will be forced to stop moving by software. In addition, the subjects could cut off the power through the emergency switch button. We intercepted the complete gait course of the left lower limb during the swing phase. The video capture of the human experiment is shown in Fig. 13. The time of a complete gait cycle is 3.5 s. The experiment demonstrates that the exoskeleton robot can effectively assist the human body to realize stable walking.
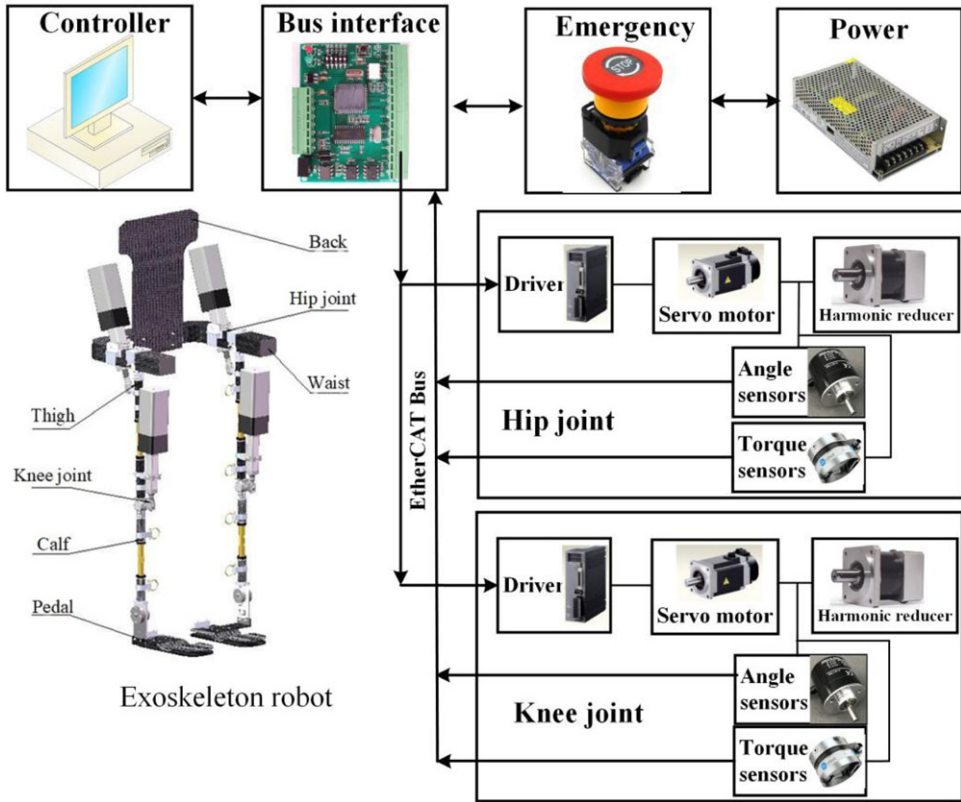
Figure 12. *The exoskeleton robot platform.*
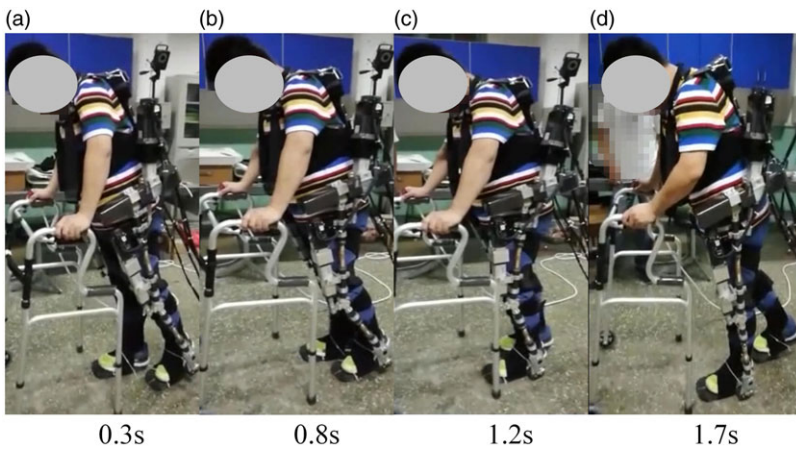
Figure 13. *Video screenshots of the human experiment.*

5.2. Human-machine system testing

A current safety threshold is set to ensure the safety of the contact force between the exoskeleton and the subject. When the human-machine contact force makes the current within the threshold value, the movement of the joint does not stop. When the contact force exceeds the current threshold, the joint stops moving. When the human-machine contact force becomes larger, the joint torque of the exoskeleton
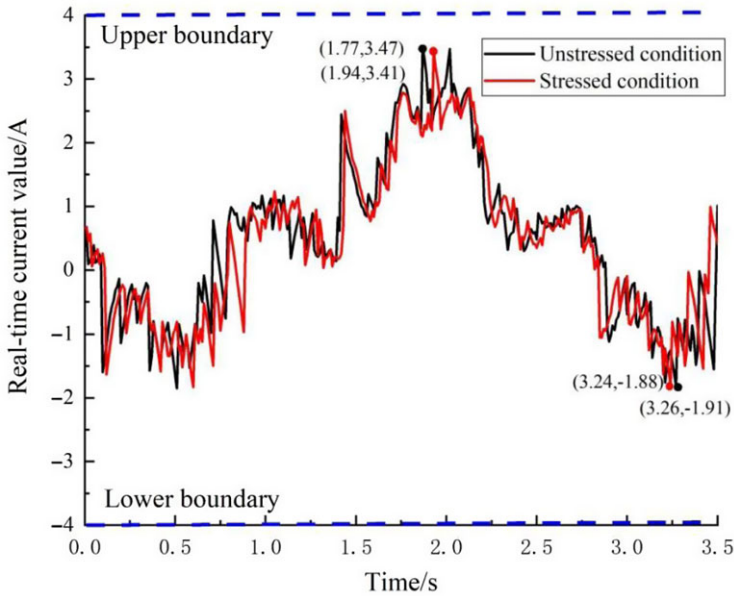
Figure 14. *Real-time currents in hip joint when in stressed and unstressed conditions.*

will be correspondingly larger to resist the obstructive force exerted by the human body, and the current output will become larger at this time. The system simultaneously detects whether the current of each joint exceeds the threshold. According to the relationship between torque and power of servo motor,

$$\tau_m = \frac{9550P}{n} \tag{37}$$

where P is the power of motor, $P = UI$, U is voltage of motor, I is current of motor. n is rational speed of motor. The current is proportional to the torque. The excessive torque output may cause secondary injury to the wearer. Generally, the torque required for joint movement does not exceed 200 N.m. According to the ammeter test, when the torque value reaches 200 N.m, the current value is about 4A. Hence, the current safety threshold was set as 4A.

We conducted experiments on the exoskeleton under conditions of unloaded(red line) and loaded(black line). The real-time current value of hip joint and knee joint are shown in Figs. 14 and 15, respectively. When the exoskeleton is in continuous contact with the subject, the current value will increase with the contact force (resistance torque) compared to the unstressed condition. We found that the current was not exceeded the current safety threshold during the entire gait cycle, indicating that the coupling performance of the human-machine system was good. To test the system's safety, we let the subject deliberately increase the range of hip joint motion to increase the human-machine contact force. Then, the joint will stop at the point S when the current generated by the contacted force exceeds the threshold value, just as shown in Fig. 15. The test ensures the safety of the exoskeleton system.

We analyzed the variation of the human joint torque, exoskeleton joint torque, and human-machine interaction torque, respectively, and the experimental results are shown in Figs. 16 and 17. It can be seen that the torque output curves of the exoskeleton and the human remain the same trend under the action of the proposed controller in this study. And the human torque always remains at a lower torque output, which is due to the exoskeleton robot compensating the required torque of the human body. It is worth noting that at 1.5 s, the human knee joint torque increases suddenly, and the exoskeleton joint torque decreases sharply, which is because the exoskeleton robot's motion control has a specific time delay behavior at the moment of phase transition and fails to make the symbolic human intention action in time. At this time, the human-machine interaction torque also increases accordingly.
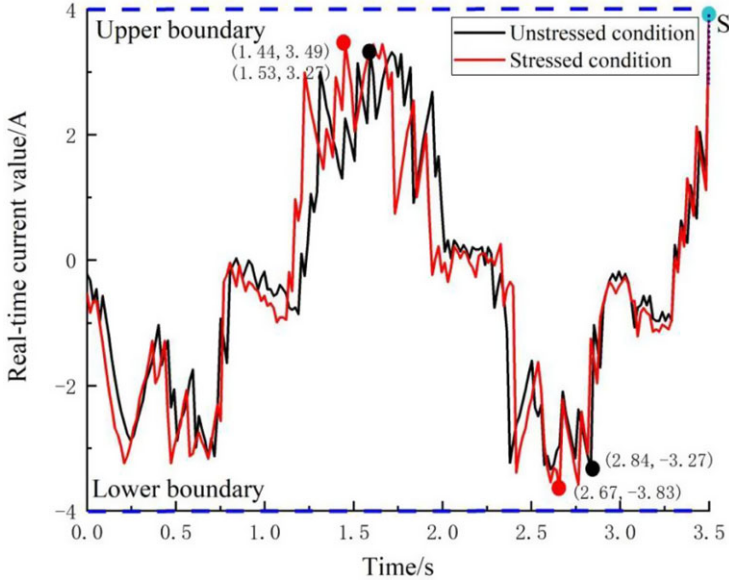
Figure 15. *Real-time currents in knee joint when in stressed and unstressed conditions.*
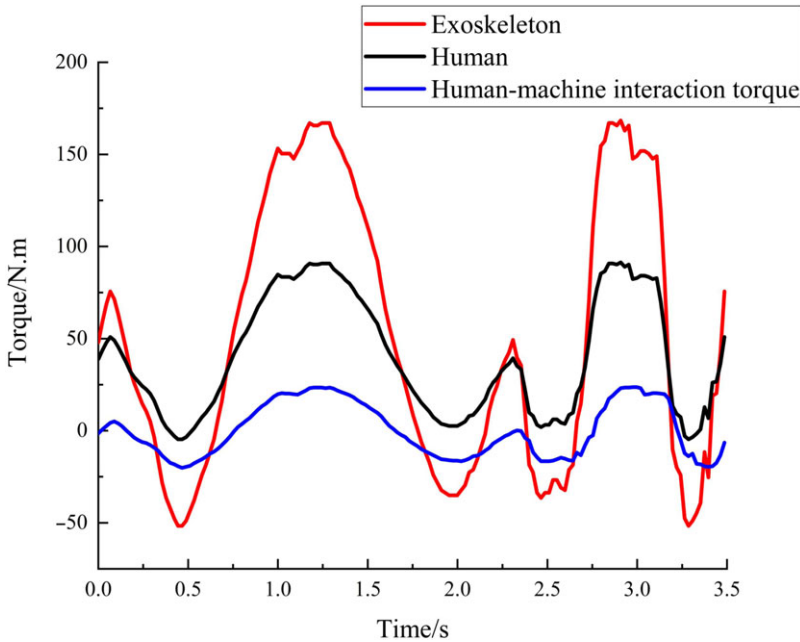

Figure 16. *Torque value of hip joint.*

We found that this situation cannot be avoided after several experiments, which is the critical problem we will solve next. The overall tendency is smooth in term of the human-machine interaction torque, and the average values of interaction torque of hip joint and knee joint are 3.215 and 2.374 N.m, indicating that the control algorithm proposed in this study can achieve stable and smooth walking.
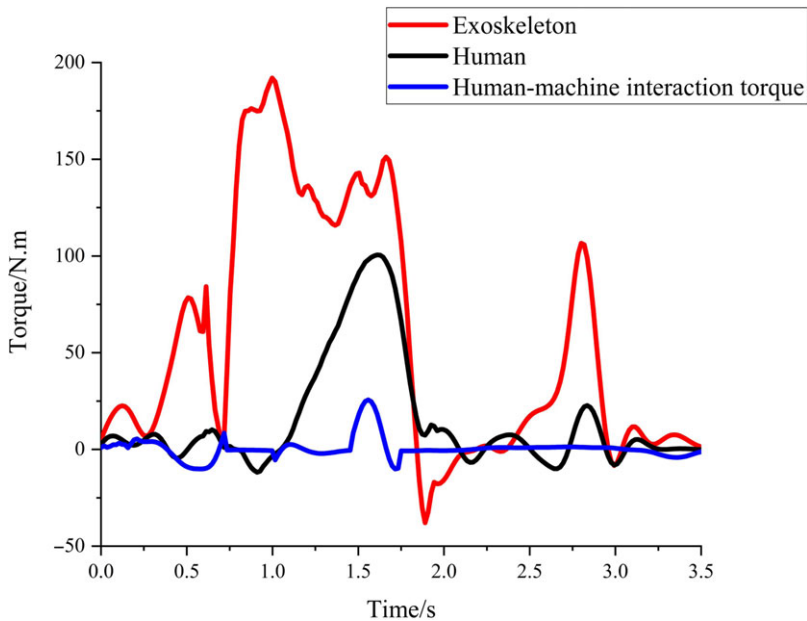
Figure 17. *Torque value of knee joint.*

6. Conclusion

In the actual rehabilitation exercise process, the movement between the lower limb rehabilitation exoskeleton and the patient must not be completely consistent, which makes the interaction force between the exoskeleton robot and the patient, and the compliance control can reduce the interaction force between the exoskeleton robot and the patient. In this study, a 6 DoFs exoskeleton robot is designed, and the exoskeleton dynamics analysis is conducted. A human-machine coupling model of the exoskeleton robot based on the spring-damping model was established. To meet the needs of patients' rehabilitation training, a fuzzy radial impedance (RBF-FVI) controller is proposed to satisfy human motion laws. The controller includes a fuzzy position control module and an outer-loop impedance control module. Through simulation experiments, it is demonstrated that the control method proposed in this research is significantly better than other traditional control methods in trajectory following. In this study, human-machine wear experiments are conducted. The experimental results show that the exoskeleton robot system designed in this study can assist the human body to achieve stable and smooth walking. According to the experimental results, there is a sudden change of torque during the gait phase transition, which requires further optimization of the exoskeleton robot structure and control method. This will be our future research priority. In addition, we also plan to conduct human-machine experiments on stroke patients to further validate the effectiveness of the robotic system designed in this study.

References

[1] X. Zhao, X. Tan and B. Zhang, "Development of soft lower extremity exoskeleton and its key technologies: A survey," *Robot* **42**, 365–384 (2020).

[2] R. Bogue, "Robotic exoskeletons: A review of recent progress," *Ind. Robot.* **42**(1), 5–10 (2015).

[3] de Looze, M. P., T. Bosch and F. Krause, "Exoskeletons for industrial application and their potential effects on physical work load," *Ergon* **59**, 671–681 (2015).

[4] G. Zhang, G. Liu and S. Ma, "Biomechanical design of escalading lower limb exoskeleton with novel linkage joints," *Technol. Health Care* **25**(9), 267–273 (2017).

[5] M. Mokhtari, M. Taghizadeh and M. Mazare, "Hybrid adaptive robust control based on CPG and ZMP for a lower limb exoskeleton," *Robotica* **39**(2), 181–199 (2021).

[6] P. Zhang and J. Zhang, "Lower limb exoskeleton robots' dynamics parameters identification based on improved beetle swarm optimization algorithm," *Robotica* **40**(8), 2716–2731 (2022).

[7] P. Zhang and J. Zhang, "Motion generation for walking exoskeleton robot using multiple dynamic movement primitives sequences combined with reinforcement learning," *Robotica* **40**(8), 2732–2747 (2022).

[8] C. Ferraresi, G. G. Muscolo, C. De Benedictis, M. Paterna and S. M. Gisolo, Design and modeling of a novel pneumatic passive upper limb exoskeleton based on McKibben artificial muscle (2021).

[9] B. Penzlin, "Design and first operation of an active lower limb exoskeleton with parallel elastic actuation," *Actuators* **10**(4), 75 (2021).

[10] X. Cao and W. Wu, "Research on impact resistance and active-passive compliance control of rope-driven joint unit," *J. Braz. Soc. Mech. Sci.* **43**(9), 1–21 (2021).

[11] W. Qian, L. Ai, Z. Zhou, J. Liao, X. Xiao and Z. Guo, "Adaptive Impedance Control of A 6-DOF Cable-Driven Compliant Upper Limb Rehabilitation Robot," **In:** *2021 27th International Conference on Mechatronics and Machine Vision in Practice (M2VIP)*(IEEE, 2021).

[12] H. Y. Lee, J. H. Park and T.-W. Kim, "Comparisons between Locomat and Walkbot robotic gait training regarding balance and lower extremity function among non-ambulatory chronic acquired brain injury survivors," *Medicine* **100**(18), e25125 (2021).

[13] Z. Li, Y. Yuan, L. Luo, W. Su, K. Zhao, C. Xu and M. Pi, "Hybrid brain/muscle signals powered wearable walking exoskeleton enhancing motor ability in climbing stairs activity," *IEEE Trans. Med. Robot. Bion.* **1**(4), 218–227 (2019).

[14] H. Kazerooni, "The Berkeley lower extremity exoskeleton," *J. Dyn. Syst.-T ASME* **128**, 9–15 (2006).

[15] Ekso Bionics (2013), http://www.eksobionics.com/ekso.

[16] L. Chen, C. Wang, X. Song, J. Wang, T. Zhang and X. Li, "Dynamic trajectory adjustment of lower limb exoskeleton in swing phase based on impedance control strategy," *Proc. Inst. Mech. Eng. I J. Syst. Cont. Eng.* **234**(10), 1120–1132 (2020).

[17] L. Luna, I. García, M. Mendoza, G. Dorantes-Méndez, A. Mejía-Rodríguez and I. Bonilla, "EMG-Based Kinematic Impedance Control of A Lower-Limb Exoskeleton," **In:** *Latin American Conference on Biomedical Engineering* (Springer, Cham, 2019).

[18] Y. Wang, "An Impedance Control Method of Lower Limb Exoskeleton Rehabilitation Robot Based on Predicted Forward Dynamics," **In:** *2020 IEEE 19th International Conference on Trust, Security and Privacy in Computing and Communications (TrustCom)* (IEEE, 2020).

[19] M. Mokhtari, M. Taghizadeh and M. Mazare, "Impedance control based on optimal adaptive high order supertwisting sliding mode for a 7-DOF lower limb exoskeleton," *Meccanica* **56**(3), 535–548 (2021).

[20] J. Chen, Y. Li and J. Zeng, "Active interactive genetic control for lower limb rehabilitation robots with uncertainties," **In:** *2021 40th Chinese Control Conference (CCC)* **40**, 491–496 (2021). doi: 10.23919/CCC52363.2021.9549638.

[21] W. Huo, H. Moon, M. A. Alouane, V. Bonnet, J. Huang, Y. Amirat and S. Mohammed, "Impedance modulation control of a lower-Limb exoskeleton to assist sit-to-stand movements," *IEEE Trans. Robot.* **38**(2), 1230–1249 (2021).

[22] I. Sharp, F. Huang and J. Patton, "Visual error augmentation enhances learning in three dimensions," *J. Neuroeng. Rehabil.* **8**(1), 1–6 (2011).

[23] E. Akdoğan, E. Taçgin and M. A. Adli, "Knee rehabilitation using an intelligent robotic system," *J. Intell. Manuf.* **20**(2), 195–202 (2009).

[24] Z. Chen, Q. Guo, Y. Yan and Y. Shi, "Model identification and adaptive control of lower limb exoskeleton based on neighborhood field optimization," *Mechatronics* **81**(2), 102699 (2022).

[25] W. Qian, L. Ai, Z. Zhou, J. Liao, X. Xiao and Z. Guo, "Adaptive Impedance Control of A 6-DOF Cable-Driven Compliant Upper Limb Rehabilitation Robot," **In:** *2021 27th International Conference on Mechatronics and Machine Vision in Practice (M2VIP)* (IEEE, 2021).

[26] B. Baigzadehnoe, Z. Rahmani, A. Khosravi and B. Rezaie, "On position/force tracking control problem of cooperative robot manipulators using adaptive fuzzy backstepping approach," *ISA Trans.* **70**(10), 432–444 (2017).

[27] Dániel Stojcsics, "Fuzzy Controller for Small Size Unmanned Aerial Vehicles," **In:** *2012 IEEE 10th International Symposium on Applied Machine Intelligence and Informatics (SAMI)* (IEEE, 2012).

[28] Z. Li, X. Li, Q. Li, H. Su, Z. Kan and W. He, "Human-In-the-Loop control of soft exosuits using impedance learning on different terrains," *IEEE Trans. Robot.*, early access, 1–15 (2022).

[29] X. Yu, B. Li, W. He, Y. Feng, L. Cheng and C. Silvestre, "Adaptive-constrained impedance control for human-robot co-transportation," *IEEE Trans. Cybern.*, early access, 1–13 (2021).

[30] B. Brahmi, M. Driscoll, I. K. El Bojairami, M. Saad and A. Brahmi, "Novel adaptive impedance control for exoskeleton robot for rehabilitation using a nonlinear time-delay disturbance observer," *ISA Trans.* **108**, 381–392 (2021).

[31] P. Zhang, J. Zhang and Z. Zhang, "Design of RBFNN-based adaptive sliding mode control strategy for active rehabilitation robot," *IEEE Access* **8**, 155538–155547 (2020).

[32] J. Zhang, C. C. Cheah and S. H. Collins, "Experimental Comparison of Torque Control Methods on an Ankle Exoskeleton During Human Walking," **In:** *2015 IEEE International Conference on Robotics and Automation (ICRA)* (IEEE, 2015).

[33] H. Li, C. Liu, L. Yan, B. Zhang, D. Li and Q. Zhang, "Impedance control and joint test study of upper limb exoskeleton robot," *J. Mech. Eng.* **56**(19), 200–209 (2020).

[34] Y. M. Zhang, Q. C. Wu, B. Chen, H. T. Wu and H. R. Liu, "Fuzzy neural network impedance control of a soft rehabilitation exoskeleton robot for lower limbs," *Robotics* **42**, 477–484 (2020).